IRANIAN JOURNAL OF CATALYSIS

Catalytic activity of immobilized Ag and Pd nanoparticles on the magnetic natural zeolite using *Chrysanthemum morifolium* flower extract in the reduction/decolorization of dyes

Akbar Rostami-Vartooni*[a], Leila Rostami[a], Mojtaba Bagherzadeh*[b]

a) Department of Chemistry, Faculty of Science, University of Qom, Qom 3716146611, Iran
b) Reactor and Nuclear Safety School, Nuclear Science and Technology Research Institute, 81465-1589, Isfahan, Iran .

Received 5 May 2021; received in revised form 4 July 2021; accepted 16 July 2021

ABSTRACT

In this study, Ag and Pd nanoparticles (NPs) were immobilized on natural zeolite and magnetized zeolite (Fe_3O_4/natural zeolite) by using an aqueous *Chrysanthemum morifolium* flower extract, as a green and low-cost method. Different techniques such as FTIR, XRD, FESEM, EDS, and VSM were used for the characterization of prepared nanocomposites. The FESEM and TEM images of nanocomposites showed that the quasi-spherical Ag and Pd NPs with mostly 20–50 nm particles size have successfully formed and are well dispersed on the supports surface. The effect of various parameters such as nanocomposite type, initial dye, $NaBH_4$ concentrations, catalyst dose, and pH were studied in the catalytic reduction/decolorization of three organic dyes. In the absence of $NaBH_4$ or catalyst, no color changes were observed even after 90 min. The reduction rates of the selected dyes in the presence of stable catalysts were found to be in an order of Pd/Fe_3O_4/natural zeolite > Pd/natural zeolite > Ag/Fe_3O_4/natural zeolite > Ag/natural zeolite > Fe_3O_4/natural zeolite.

***Keywords**: Natural zeolite; Heulandite; Fe_3O_4 nanocomposites; C. morifolium; Catalytic reduction; Decolorization*

1. Introduction

Nowadays, nanotechnology plays an essential role in different sectors such as health, agriculture, energy, and the environment [1-3]. In this field, metal nanoparticles (MNPs) can be used as efficient catalysts for many organic reactions, since they have high surface area [4-7]. Among all the MNPs, Ag and Pd NPs have been attracted because of their high catalytic activity, good conductivity, and stability [8, 9]. When MNPs are distributed over the surface of inorganic supports such as seashell [10], perlite [11], Fe_3O_4 [12, 13], TiO_2 [14], and ZrO_2 [7, 15], the stability and reactivity of nanoparticles are increased and their separation from reactions' medium is facilitated.

Some conventional methods containing chemical and physical approaches have been employed for the preparation of various MNPs but they offer the utilization of hazardous reagents or solvents and rough working conditions [16, 17].

*Corresponding author:
E-mail address: a.rostami127@yahoo.com and a.rostami@qom.ac.ir (**A. Rostami-Vartooni**) *mjmo123@yahoo.com* (**M. Bagherzadeh**)

Up to now, different MNPs have been synthesized using several aqueous plant extracts [18-20]. This economical friendliness and simple synthesis method occurred in the presence of a non-toxic solvent or reducing and stabilizing agents under gentle reaction conditions.

Chrysanthemum morifolium as an ornamental and traditional plant is useful for insomnia, headaches, hyperglycemia, and eye diseases. Extracts of this plant have potent neuroprotective [21, 22], cardiovascular protective [23], anti-inflammatory [24], antioxidant [25, 26], anti-tumor [27], anti-HIV [28] effects due to the presence of flavonoids, triterpenoids, monoterpenes, sesquiterpenes and other antioxidant constituents [29, 30].

Natural and synthesized zeolites with a three-dimensional (3-D) network of $[SiO_4]^{4-}$ and $[AlO_4]^{5-}$ tetrahedrons have been widely used for various fields including human health, filtration of drinking water, animal nutrition, gas purification in industry, agriculture, and construction [31, 32]. Since these inorganic materials have high storage capacity, large

thermal stability, and unique framework structures with exchangeable cations, micropores, and channels, they have been applied as beneficial catalysts and adsorbents for heavy metals, nuclear elements or organics [33-36]. There are more than 45 different types of known natural zeolites with slightly different compositions such as heulandite, phillipsite, mordenite, and chabazite [37]. The heulandite (or HEU topology) as the most abundant natural zeolites is found with a Si/Al ratio ranging between 3-5. These natural minerals contain a ten-member ring channel pore system with eight-member ring cross-channels. The higher silica member of this family is named clinoptilolite; its thermal stability and Si/Al ratio are different from heulandite. The Si/Al ratio of clinoptilolite is greater than 4. Natural zeolites can be used as supports for the preparation of catalysts because of their availability, low toxicity and cost, high safety, small cavities, and environmental stability properties [38, 39].

Azo dyes have been recognized as the most critical and strategic water and wastewater pollutants, which are produced by industrial processes. These compounds are very harmful to humans and animals, due to their carcinogenic and mutagenic properties [40-42]. Many different methods have so far been implemented to remove pollutants from the effluent system including adsorption, chemical reduction, photodegradation, ion exchange, coagulation, and membrane separation [43-55]. The reduction/decolorization process in the presence of $NaBH_4$ as a reducing agent converts the hazardous materials to less toxic organic compounds. In this process, the Ag and Pd NPs**,** due to their appropriate redox potentials, can facilitate the electron transfer between the borohydride ions (donor) and dye molecule (acceptor) to overcome the kinetic barrier.

According to the literature information, no report has been found on the application of *C. morifolium* for the preparation of nanocomposites. Therefore, in this study the Ag and Pd NPs were synthesized on the natural zeolite and magnetically recoverable Fe_3O_4/natural zeolite surfaces during using *C. morifolium* flower extract. Finally, the biosynthesized catalysts were used in the reduction reactions of MB, MO, and RhB organic dyes.

2. Experimental

2.1. Materials and methods

All the materials were purchased from Merck (Darmstadt, Germany). Heulandite sample as a natural zeolite was collected from manzarieh zeolite mine (Qom, Iran). The *C. morifolium* flowers were collected from the north of Isfahan, Iran (Vartoon village). UV-Vis spectra were acquired using a Lambda-35 UV-Vis spectrophotometer (PerkinElmer, United States). The functional groups of the prepared natural zeolite nanocomposites were investigated using Fourier transform infrared (FT-IR) spectra obtained on a Cary 630 FTIR spectrometer between 400 and 3900 cm^{-1}. The phase compositions of the natural zeolite and its nanocomposites were identified by a Philips PW 1730 X-ray diffractometer by Cu-Kα radiation (λ = 0.1541 nm) with scanning range from 10° to 80°. XRF analysis of the natural zeolite was done with Bruker, S4 instrument. The morphological characterization of the synthesized Ag and Pd nanocomposites of natural zeolite was examined through a transmission electron microscope (TEM, Philips-EM-208S) and field emission scanning electron microscope (FESEM, Cam scan MV2300) equipped with energy-dispersive X-ray spectroscopy (EDS). Vibrating sample magnetometer (VSM) measurement of the synthesized Fe_3O_4/natural zeolite nanocomposite was taken by a Quantum Design MPMS XL SQUID magnetometer.

2.2. Preparation of aqueous C. morifolium flower extract

30 g of dried flowers of *C. morifolium* was mixed with 150 mL of DI water and then heated at 60 °C. After 30 min the resulting aqueous flower extract was filtered by using a Whatman filter paper No. 1. Afterwards, this aqueous extract was used for the reduction of Ag+ and Pd^{2+} ions to Ag and Pd NPs on the surfaces of natural zeolite and its Fe_3O_4 nanocomposite.

2.3. Synthesis of Fe_3O_4/natural zeolite nanocomposite by co-precipitation method

2 g of natural zeolite was mixed with a solution of 2 M NaOH (180 mL). A homogeneous solution containing $FeCl_2{\cdot}6H_2O$ (20 mL, 1.0 M), $FeCl_3{\cdot}6H_2O$ (20 mL, 2.0 M), and HCl (20 mL, 2.0 M) was then added dropwise to the prepared basic mixture of the zeolite under an argon atmosphere and vigorous stirring for 30 min. Finally, the formed Fe_3O_4/natural zeolite by using an external magnet was separated, washed with de-ionized water, and dried in an oven at 80 °C.

2.4. Synthesis of Ag/natural zeolite nanocomposite

4 mL of an aqueous solution of 0.3 M $AgNO_3$ was added to a mixture containing 1.0 g natural zeolite and 20 mL of the obtained *C. morifolium* extract [19]. This heterogeneous mixture was continuously stirred for 15 min. With immobilization of Ag NPs on the support surface, the white color of the natural zeolite changes to dark color. Finally, the biosynthesized Ag/natural zeolite nanocomposite was separated, washed with de-ionized water, and dried.

2.5. Synthesis of Pd/natural zeolite nanocomposite

20 mL of the prepared flower extract of *C. morifolium* was added to an aqueous suspension of natural zeolite (1.0 g) and $PdCl_2$ solution (0.2 g in 9 mL acetonitrile) under vigorous stirring for 30 min at 70 °C. Finally, the filtered Pd/natural zeolite was washed with de-ionized water and then dried.

2.6. Synthesis of Ag/Fe_3O_4/natural zeolite nanocomposite

4 mL of a solution of 0.3 M $AgNO_3$ was added to a mixture containing 1.0 g Fe_3O_4/natural zeolite and 20 mL of the prepared *C. morifolium* flower extract under stirring [19]. After 30 min, the obtained nanocomposite was washed with de-ionized water, and then dried in an oven at 80 °C.

2.7. Synthesis of Pd/Fe_3O_4/natural zeolite nanocomposite

0.2 g $PdCl_2$ solution dissolved in 9 mL acetonitrile was added to a mixture containing 1.0 g Fe_3O_4/natural zeolite and 20 mL of the *C. morifolium* flower extract. The suspension was stirred for 30 min at room temperature. After filtration, the resultant nanocomposite was washed with de-ionized water, and then dried at 80 ºC.

2.8. General procedure for reduction/decolorization of dyes

3 or 7 mg of the prepared Ag or Pd nanocomposites was added to a solution containing MB, MO, or RhB (10 ppm, 50 mL) and an aqueous solution of 5.3×10^{-3} M $NaBH_4$ (50 mL). These reduction reactions of selected dyes were stirred at ambient temperatures and then monitored by UV-Vis spectroscopy at different times at λ_{max}. The pH of the dye solutions was adjusted by adding 6 M HCl or 6 M NaOH.

3. Result and Discussion

In this study, natural zeolite and its Fe_3O_4 nanocomposite were modified by loading Ag or Pd NPs and then applied as catalysts in the reduction/decolorization of three azo dyes. The aqueous *C. morifolium* flower extract was applied for the bio reduction of Ag^+ and Pd^{2+} ions on the surface of supports. The obtained natural zeolite nanocomposites were characterized using different techniques.

3.1. Characterization of the supports and their Ag and Pd NPs

The natural zeolite composition obtained from the XRF results is summarized in **Table 1**. The Si/Al ratio of the natural sample is about 3.3, which confirms that the zeolite belongs to the heulandite type. The presence of calcite as an impurity can be confirmed by a high amount of CaO in this natural sample. FTIR spectra of this inorganic matter, Fe_3O_4/natural zeolite, and their Ag or Pd nanocomposites are seen in **Fig. 1**. The peaks appearing at about 790 and 450 cm^{-1} are related to the stretching vibrations of T–O–T bridges (T = Al or Si) and T–O bending vibration bands, respectively [56-58] [59]. The strong vibrations observed near 1040 cm^{-1} which can be related to T–O or T–O–T stretching band indicate the possibility of the presence of heulandite type zeolite. In general, heulandites have higher Al atoms in the framework tetrahedral sites in relation to clinoptilolites, and is expected that this peak to be found in lower wavelength values than in clinoptilolites [60]. The functional groups have not changed after the immobilization of Ag and Pd NPs on natural zeolite. The absorption peaks at about 1630 and 3400-3700 cm^{-1} are assigned to the bending and stretching vibrations of OH groups, respectively. FTIR spectra of synthesized Fe_3O_4 nanocomposites (**Figs. 1d-f**) have shown the Fe–O vibrations at 450-680 cm^{-1} [61]. The bands observed at about 1410, 870, and 700 cm^{-1} are assigned to the presence of calcite [62].

The observed peaks in the XRD diffraction patterns of the natural zeolite (**Fig. 2a**) are in accordance with the heulandite zeolite which contains impurities such as quartz, feldspar (albite), and calcite [63, 64]. **Figs. 2d-f** display the XRD patterns of the Fe_3O_4 nanocomposites with characteristic peaks at about 2θ = 30°, 36°, 44°, 58° and 64° which can be assigned to the (220), (311), (400), (511) and (440) crystal planes (JCPDS, No. 85-1436) [65, 66]. The peaks depicted at 2θ values of about 38°, 44°, 64.4°and 76° (**Figs. 2b** and **2e**) confirm the immobilization of biosynthesized Ag NPs on the surfaces of zeolite or its Fe_3O_4 nanocomposite. These peaks are related to the (111), (200), (220), and (311) lattice planes of face-centered cubic (*fcc*) of the Ag crystal structure (JCPDS, No. 04-0783) [10, 11]. The mean crystallite size of the Ag and Pd NPs on magnetic zeolite were calculated from the broadening of XRD peaks (patterns (e and f)), using Scherrer's formula as 14.1 and 18.3 nm, respectively [41, 47, 67].

The diffraction peaks assigned to the Pd phase have not been detected in the XRD patterns of Pd NPs/natural zeolite, possibly because the Pd loading on the surface of zeolite is not enough to form crystalline palladium [68, 69]. The Pd NPs loading on the zeolite support was 4.1 wt% determined by ICP-MS. The Pd NPs content on the Fe_3O_4/natural zeolite surface was 6.5 wt%. Therefore, new diffraction peaks in the XRD pattern of Pd/Fe_3O_4/natural zeolite (**Fig. 2f**) have appeared at 2θ = 40.1°, 46.3° and 67.8° which are indexed for the (111),.

Table 1 The XRF results of used natural zeolite.

Constituent	SiO_2	Al_2O_3	CaO	MgO	Fe_2O_3	K_2O	SrO	TiO_2	Cl	LOI*
Typical (%)	55.40	14.52	5.36	1.01	0.88	0.66	0.30	0.11	0.26	15.60

* LOI: Loss on Ignition (950 °C, 1.5h).

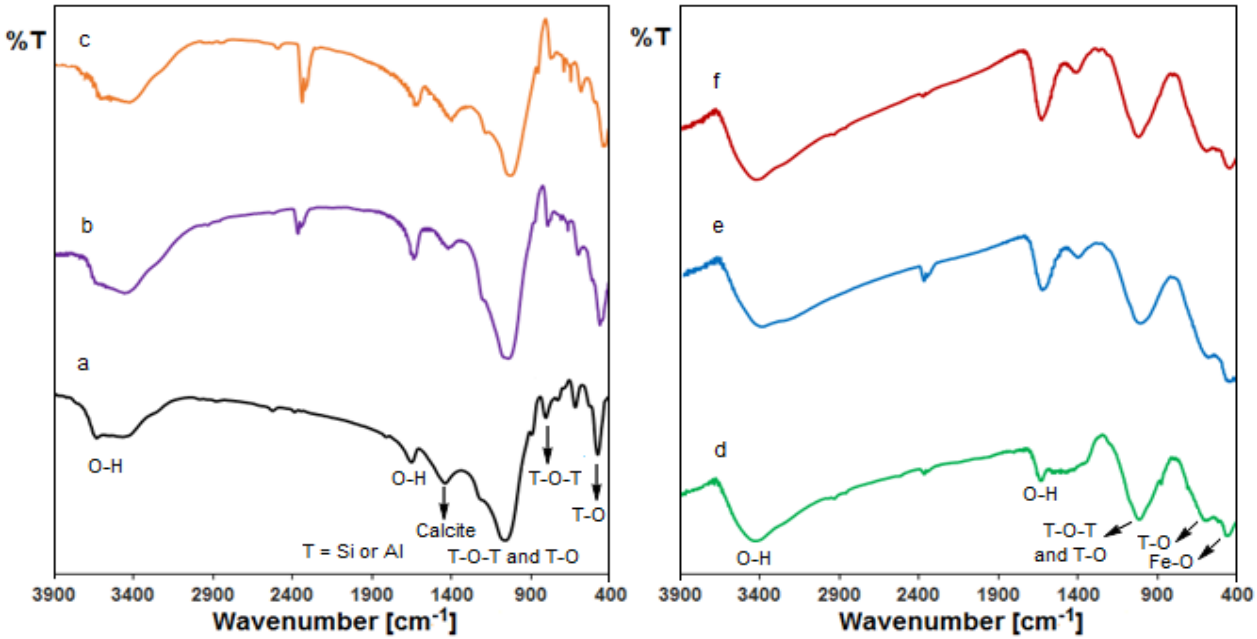

Fig. 1 FTIR spectra of the natural zeolite (a), Ag/natural zeolite (b), Pd/natural zeolite (c), Fe_3O_4/natural zeolite (d), Ag/Fe_3O_4/natural zeolite (e) and Pd/Fe_3O_4/natural zeolite (f).

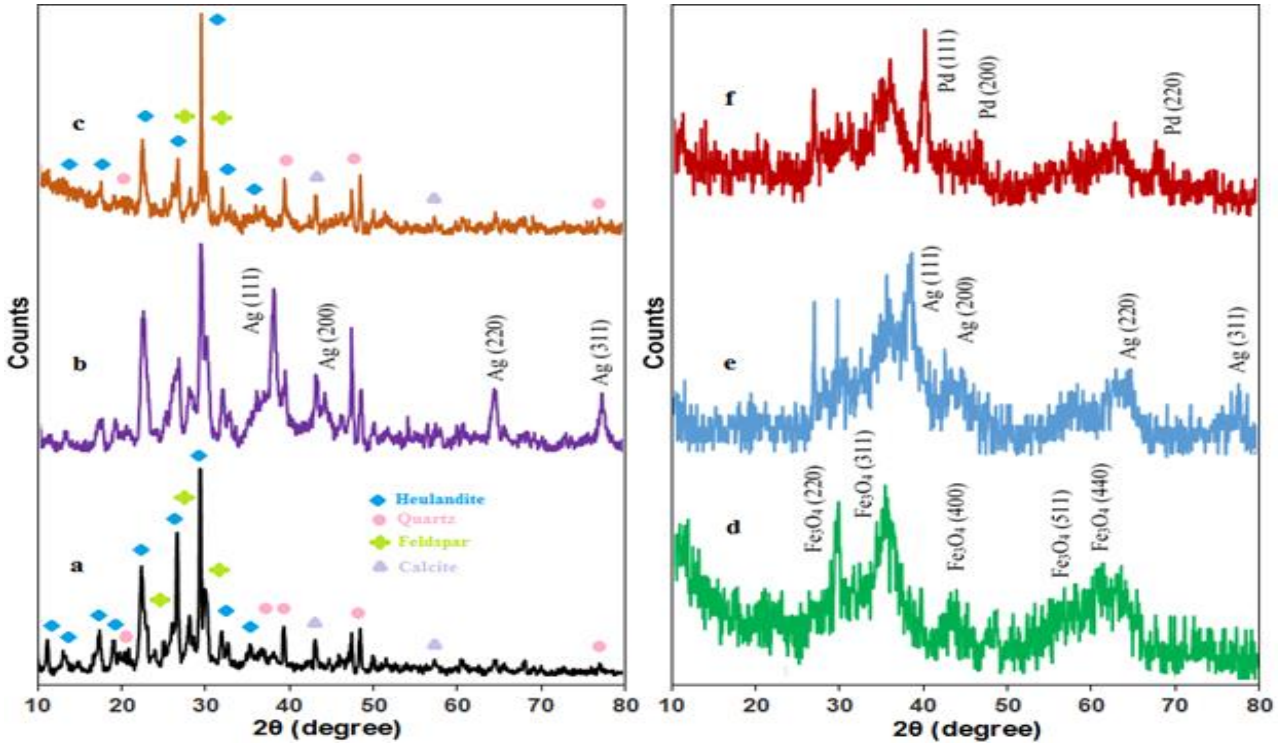

Fig. 2 X-ray powder diffractograms of the natural zeolite (a), Ag/natural zeolite (b), Pd/natural zeolite (c), Fe_3O_4/natural zeolite (d), Ag/Fe_3O_4/natural zeolite (e) and Pd/Fe_3O_4/natural zeolite (f).

(200) and (220) reflections of a *fcc* Pd crystal structure (JCPDS, No. 46-1043) [70].

The morphology and particle sizes of the Ag and Pd NPs immobilized on the natural zeolite and its Fe_3O_4 nanocomposite surfaces were further investigated by FESEM analysis. The FESEM images (**Figs. 3-6**) show the spherically shaped biosynthesized Ag and Pd NPs with mostly 20–50 nm diameters have well dispersed on the surface of natural zeolite nanocomposites and no obvious aggregation was observed. The point-scan EDS spectra in **Figs. 3c** and **5c** reveal that the atomic percentage of Ag is about 11% for Ag NPs/natural zeolite and Ag/Fe_3O_4/natural zeolite nanocomposites. According to the **Figs. 4c** and **6d**, the atomic percentage of palladium in Pd/natural zeolite and Pd/Fe_3O_4/natural zeolite nanocomposites is 3.7%, and 5.9%, respectively. The elemental mapping images of the Ag/Fe_3O_4/natural zeolite and Pd/Fe_3O_4/natural zeolite (**Fig. 7**) clearly show that the Ag or Pd NPs have successfully formed and are well dispersed on the surface of magnetically recoverable natural zeolite in the presence of aqueous *C. morifolium* flower extract.

TEM images of the Ag/Fe_3O_4/natural zeolite and Pd/Fe_3O_4/natural zeolite nanocomposites (**Fig. 8**) show the average size of quasi-spherical shape nanoparticles are about 17 and 11.5 nm, respectively. The magnetic properties of the Fe_3O_4/natural zeolite nanocomposite were determined with VSM measurement. According to the hysteresis loop of this nanocomposite (**Fig. 9**), a saturation magnetization (Ms) is around 11 emu/g. The Fe_3O_4/natural zeolite with ferromagnetic property can be conveniently separated from the reaction mixtures using an external magnet.

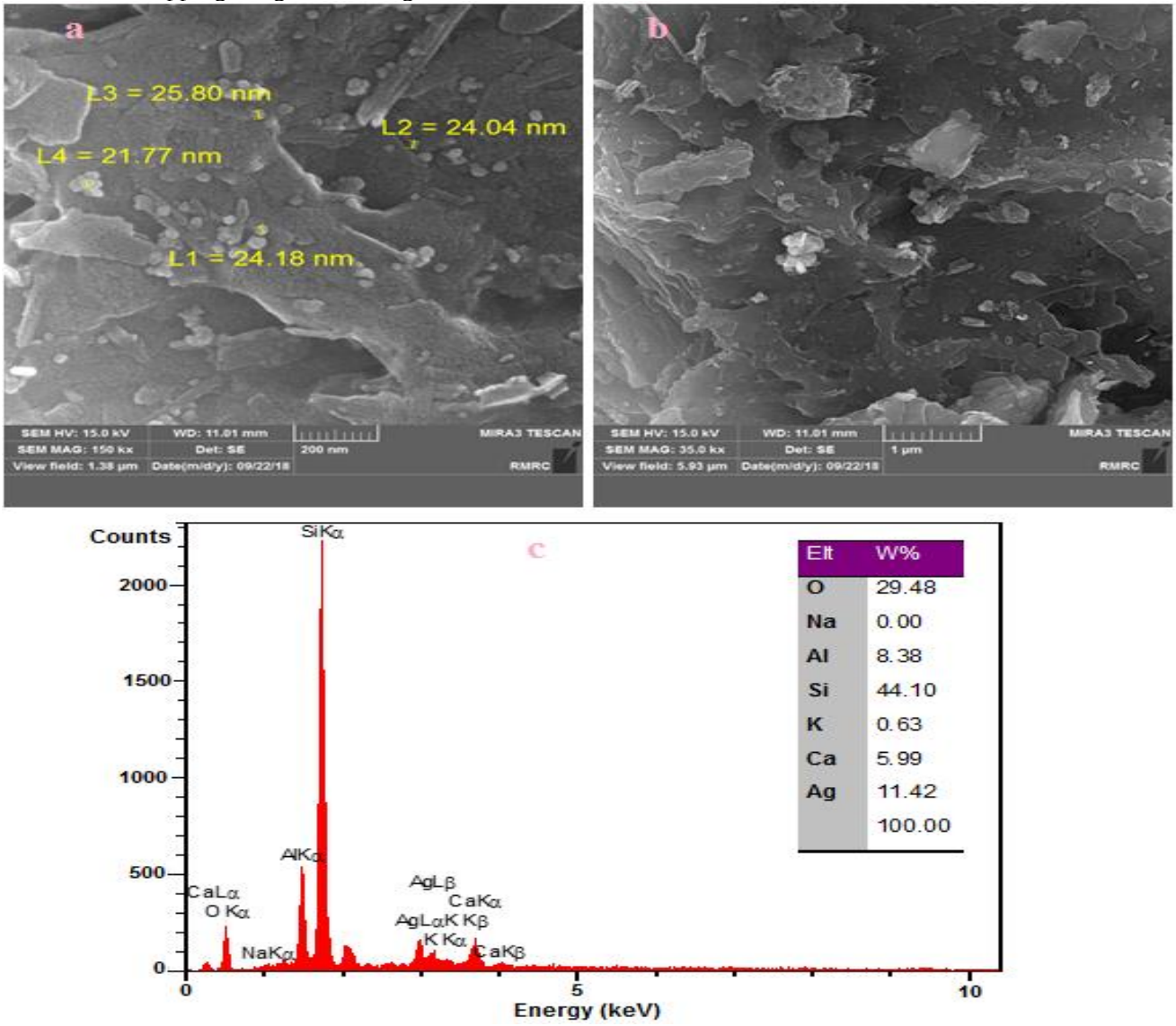

Fig. 3 (a and b) FESEM images and (c) EDS spectrum of the Ag/natural zeolite.

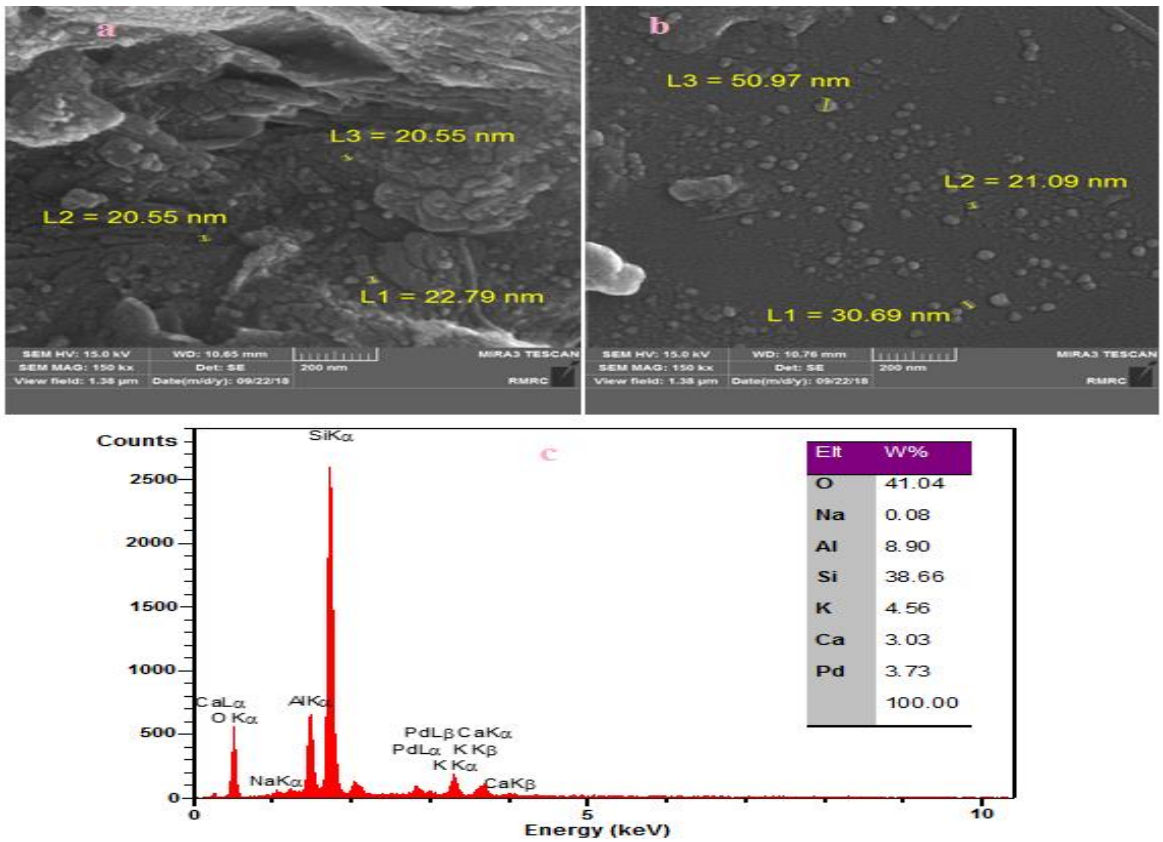

Fig. 4 (a and b) FESEM images and (c) EDS spectrum of the Pd/natural zeolite.

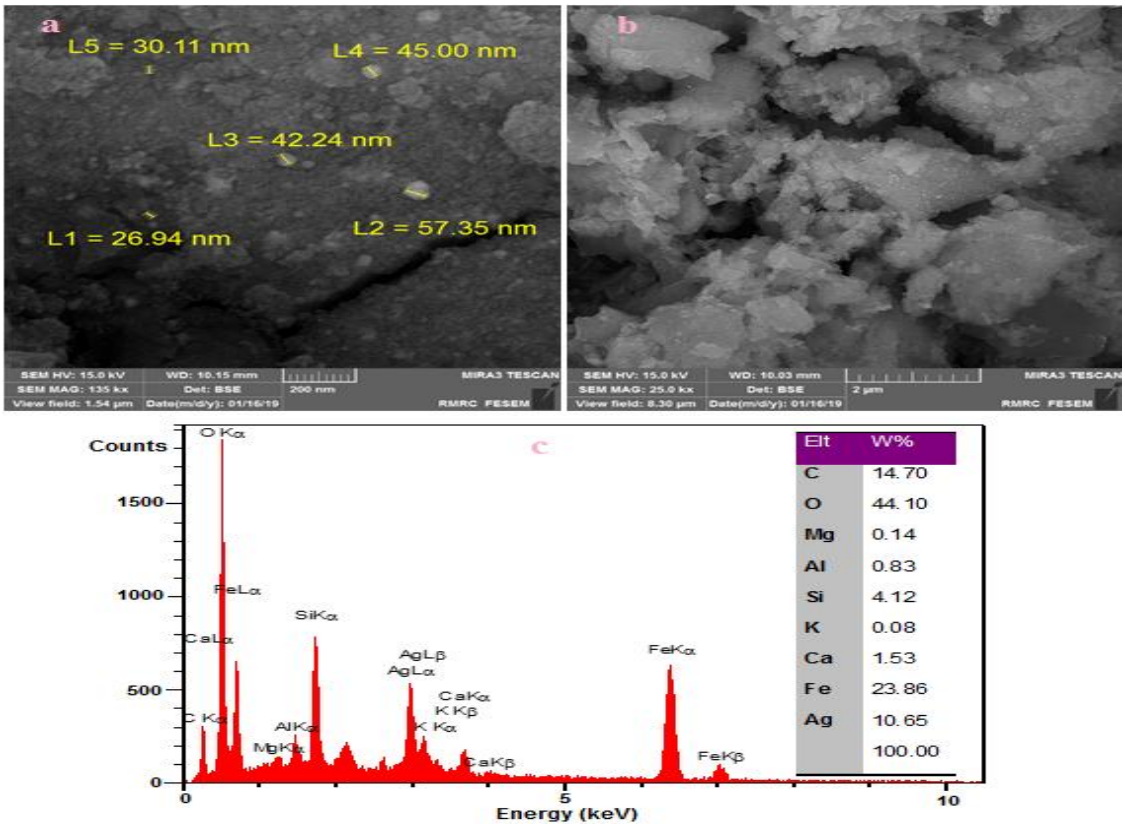

Fig. 5 (a and b) FESEM images and (c) EDS spectrum of the Ag/Fe_3O_4/natural zeolite.

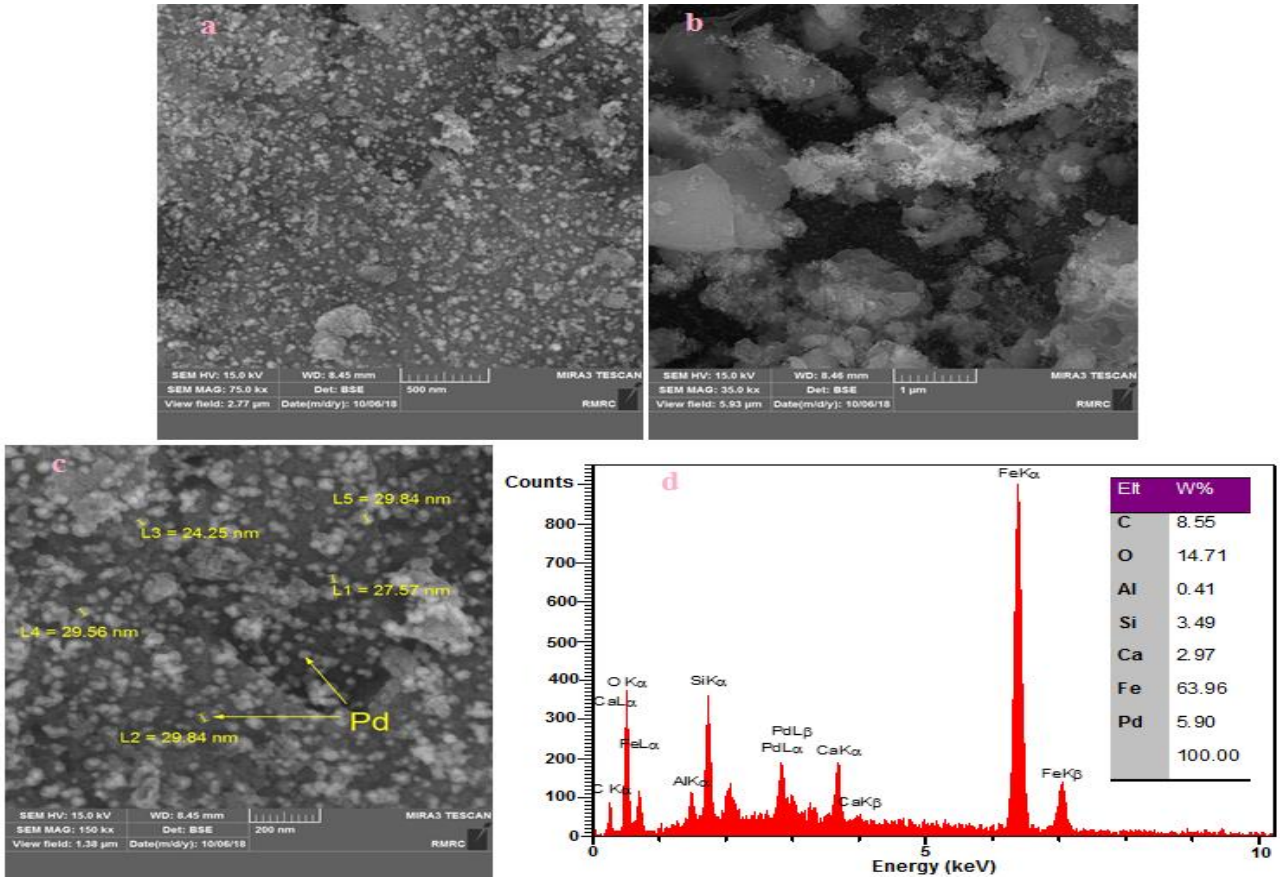

Fig. 6 (a-c) FESEM images and (d) EDS spectrum of the Pd/Fe_3O_4/natural zeolite.

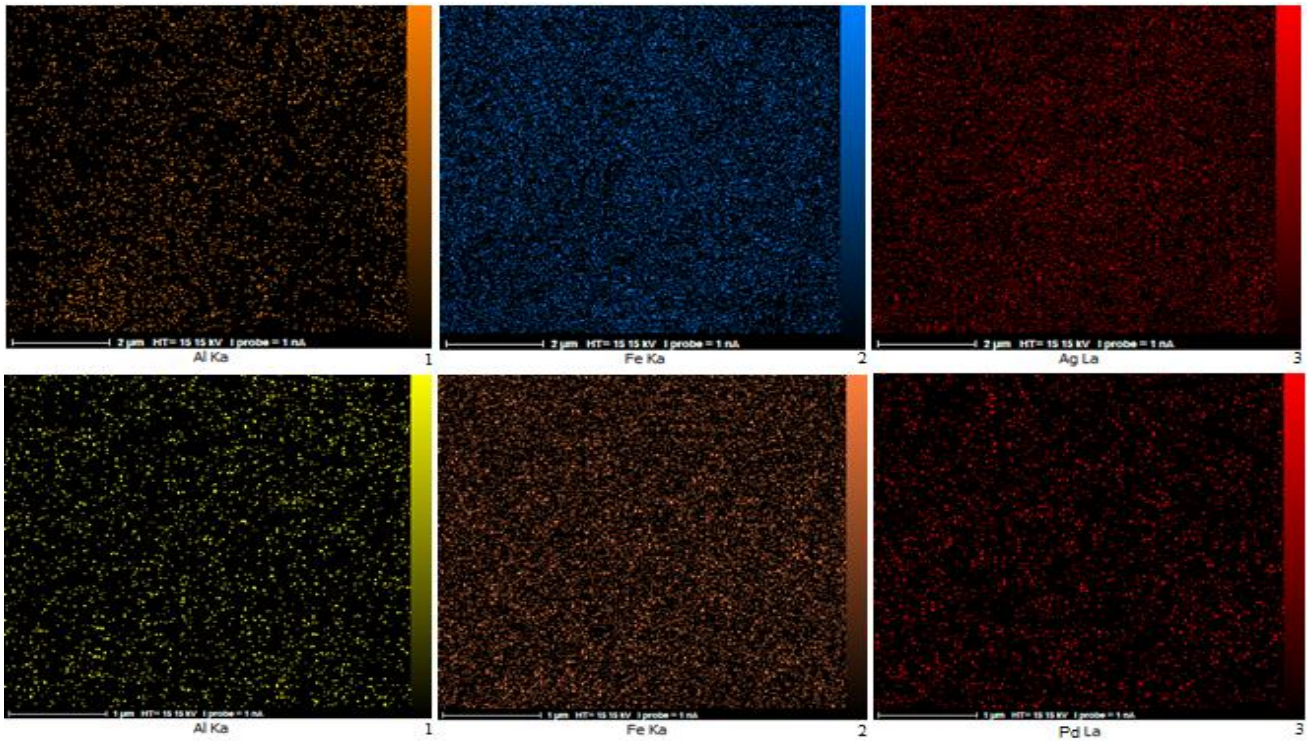

Fig. 7 Elemental mapping of the Ag/Fe_3O_4/natural zeolite (up) and Pd/Fe_3O_4/natural zeolite (down).

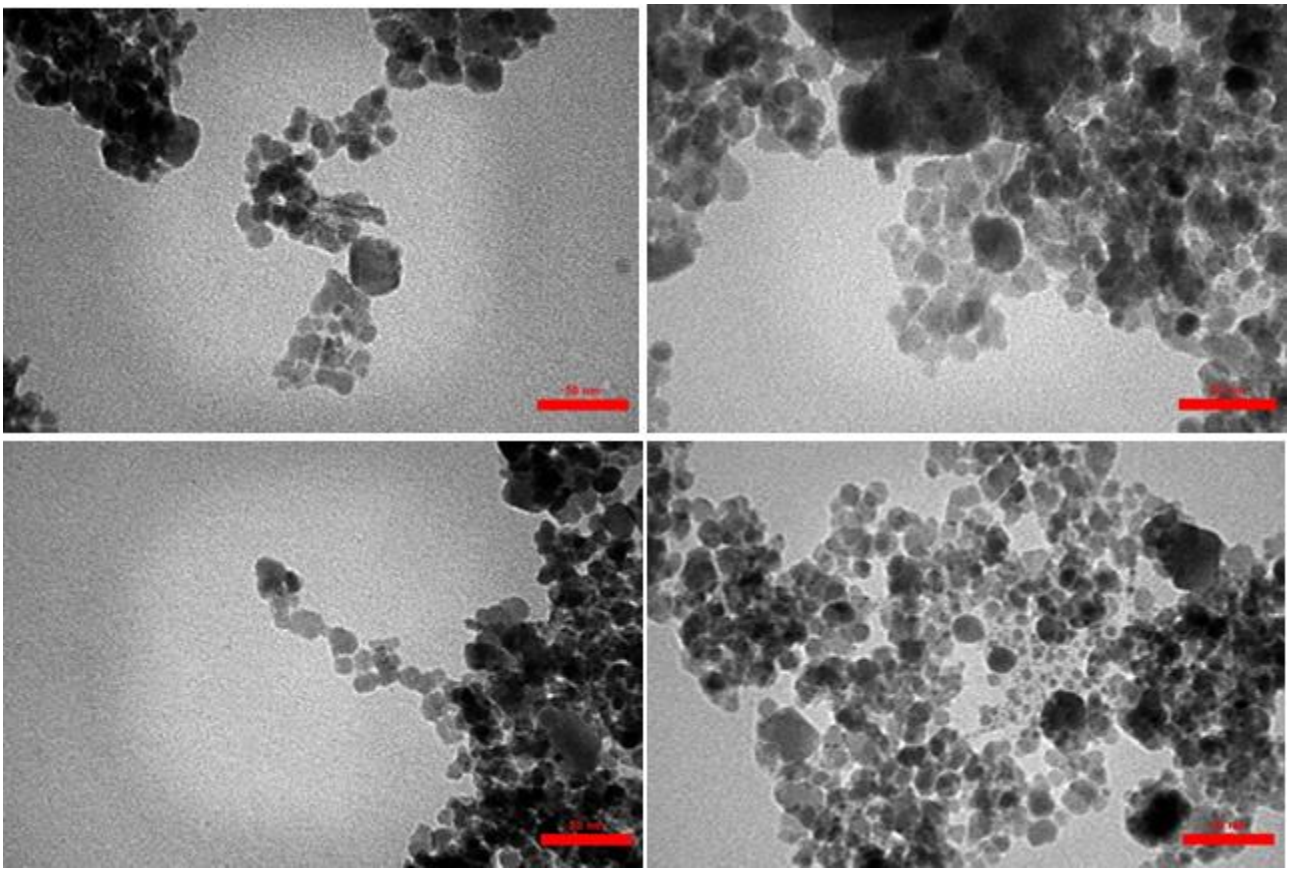

Fig. 8 TEM images of the Ag/Fe_3O_4/natural zeolite (up) and Pd/Fe_3O_4/natural zeolite (down).

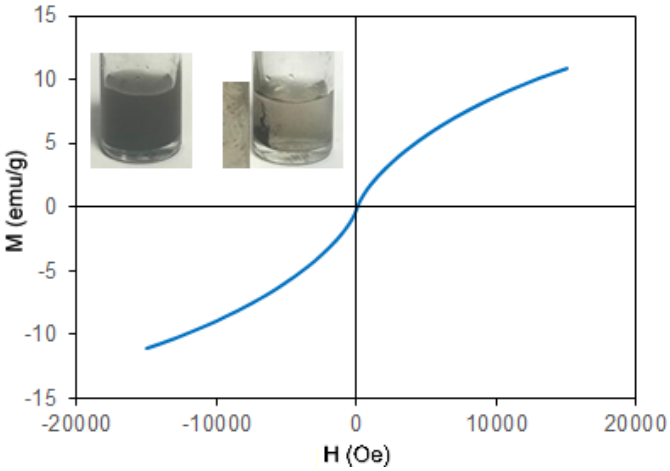

Fig. 9 Magnetization curve of the Fe_3O_4/natural zeolite nanocomposite.

3.2. Catalytic reduction/decolorization of the natural zeolite nanocomposites towards MB, MO, and RhB

The catalytic activities of the natural zeolite and its nanocomposites were evaluated for the reduction/decolorization process of MB, MO, and RhB organic dyes in the presence of $NaBH_4$ (**Scheme 1**). During the reduction/decolorization process, the colorless MO solution remains unchanged. However, the colorless MB and RhB solutions can be converted again to the initial colors. As shown in **Scheme 1**, the produced compounds in the reduction/decolorization of MO cannot be oxidized, while the reduced forms of MB and RhB can be oxidized under reaction conditions and converted to the original form. The color returning time for MB was nearly 1, 2, and 3.5 h using the Ag NPs/natural zeolite, Ag/Fe_3O_4/natural zeolite, and Pd/Fe_3O_4/natural zeolite catalysts, respectively. The colorless RhB solution returns to the initial pink color at about 9, 10.5, and 3 h using the Ag NPs/natural zeolite, Ag/Fe_3O_4/natural zeolite, and Pd/Fe_3O_4/natural zeolite, respectively. **Fig. 10** shows the changes of absorption bands during catalytic reduction at λ_{max} of 665, 464, and 553 for MB, MO, and RhB, respectively. The effects of various parameters such as initial dye and $NaBH_4$ concentrations, nanocomposite type, catalyst dose, and pH were studied and the reduction times are found in **Table 2**. The results show that , $NaBH_4$ as a strong reducing agent, cannot reduce the selected dyes even after 90 min. Also, the reduction of dyes proceeded slowly in the absence of catalysts. The decrease in the reduction/decolorization process with increasing concentration of dyes and decreasing catalyst amount

can be attributed to the limited number of available active sites on the surfaces of the catalyst. The dyes reduction rates were found to be in an order of Pd/Fe_3O_4/natural zeolite > Pd/natural zeolite > Ag/Fe_3O_4/natural zeolite > Ag/natural zeolite > Fe_3O_4/natural zeolite. The shorter times have resulted from applying modified natural zeolite by Ag and Pd NPs. The as-produced natural zeolite and Fe_3O_4/natural zeolite-supported Pd NPs catalysts have shown higher activity in the reduction process than the prepared Ag NPs nanocomposites. It seems the rate of electron transfer from BH_4^- ions to dye molecules on the Pd NPs surfaces is higher than that of Ag NPs. The solution pH is an important factor in the adsorption of dyes on the catalyst surface. The adsorption capacity of MO on the surface of the catalyst and the reduction efficiency were higher at acidic medium than those at neutral and basic conditions due to the negatively charged sulfonate groups of MO molecule [71, 72]. The adsorptive behaviors of dissolved MB and RhB in water (cationic dyes) are opposite to that of MO. In the acidic medium, the lower amount of MB adsorption and the larger reduction time were observed on the positively charged surfaces of the catalyst.

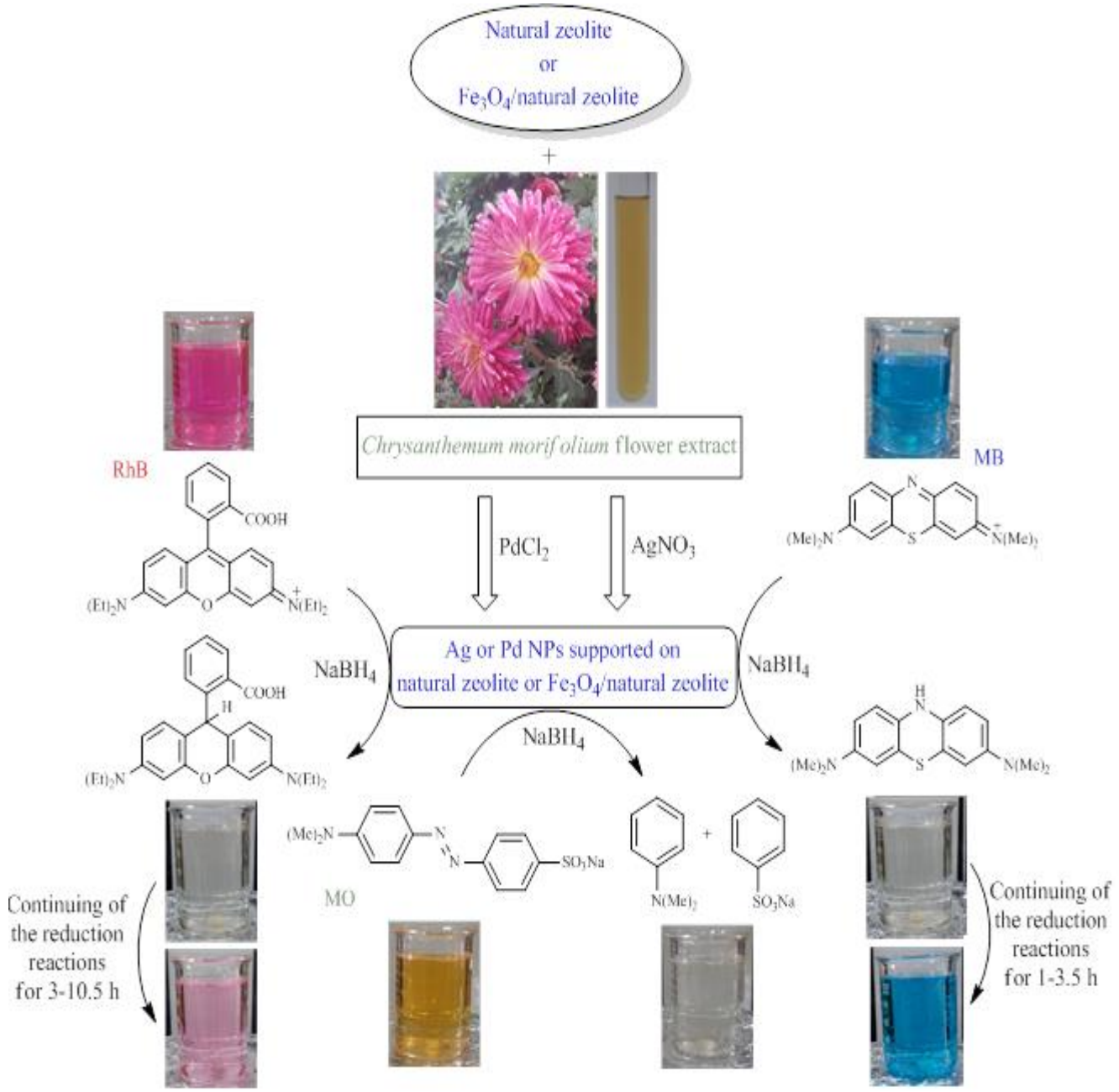

Scheme 1 Diagrammatic green preparation of natural zeolite nanocomposites and their application as catalysts for the azo dyes reduction.

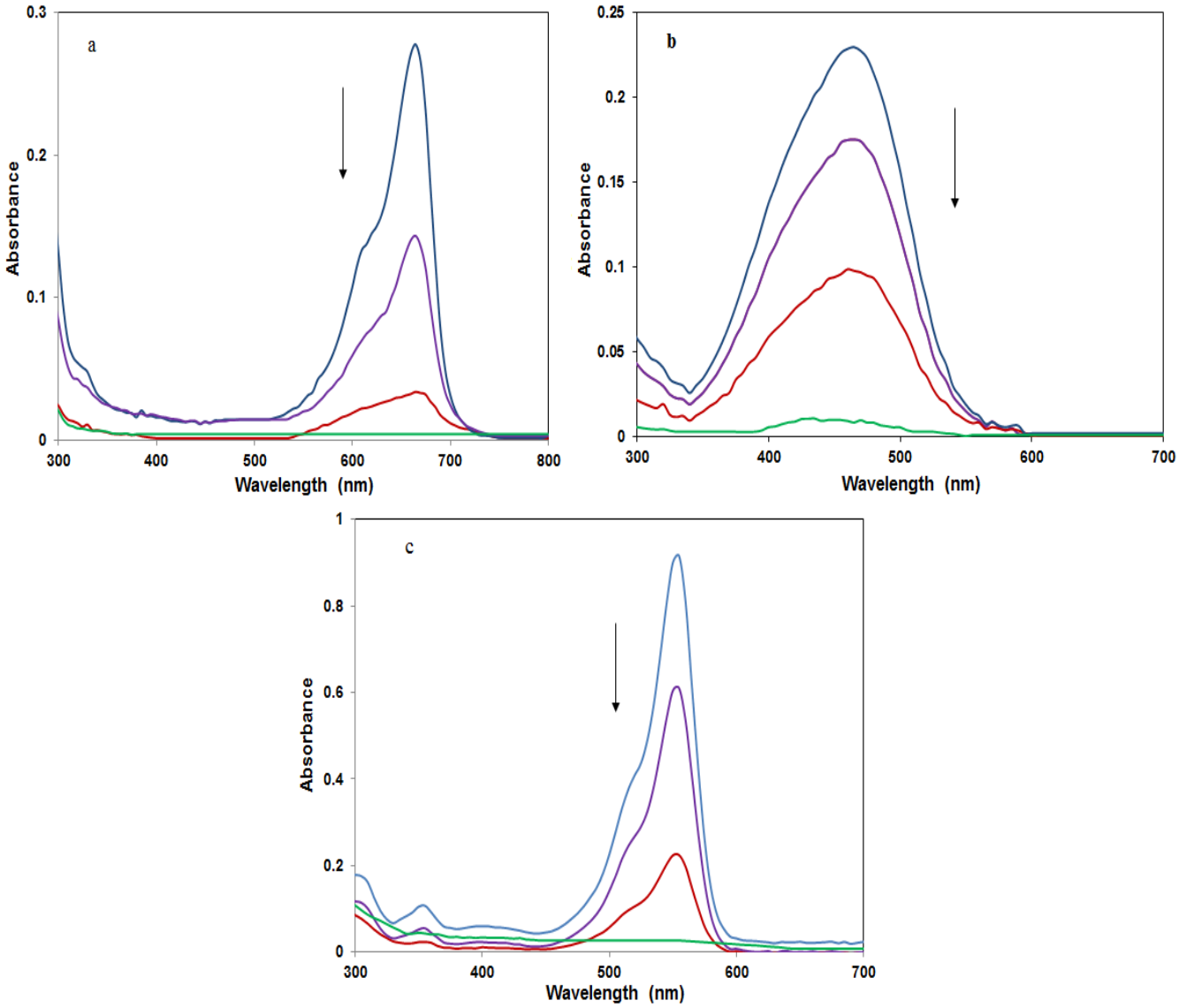

Fig. 10 The changes of UV-Vis spectra during the MB (a), MO (b), and RhB (c) reduction.

It could be found from the reduction times listed in Table 2 that the efficiency of Ag and Pd nanoparticles supported on natural zeolite or Fe_3O_4/natural zeolite nanocomposite are comparable to the reported nanocomposites in literature (Table 3) for the reduction/decolorization of textile dyes. The as-synthesized catalysts, especially Pd/Fe_3O_4/natural zeolite can efficiently perform these reduction reactions in the shortest times as promising nanocatalysts.

3.3. Reusability of catalysts

To investigate the stability and reusability of catalysts, the reduction/decolorization of MO was carried out using the recovered Ag/Fe_3O_4/natural zeolite and Pd/Fe_3O_4/natural zeolite after 4 catalytic runs. The completion time of reduction experiments does not significantly change, indicating that the prepared magnetically recoverable Ag and Pd NPs supported Fe_3O_4/natural zeolite show high catalytic stabilities, making them attractive catalysts for real catalytic applications. After further investigation, the recycled Pd/Fe_3O_4/natural zeolite catalyst was checked by FESEM, EDS (**Fig. 11**), and ICP-MS. The amount of Pd NPs loaded on recycled catalyst recorded by ICP-MS was 6.43 wt%. These obtained results display that the Pd loading and morphology of NPs are approximately unchanged on the surface of Fe_3O_4/natural zeolite after 4 catalytic runs.

Table 2 The reduction/decolorization time of azo dyes (10.0 ppm, 50 mL) using $NaBH_4$ (5.3×10^{-3} M, 50 mL) and different nanocomposites (7 mg).

Catalyst (mg)	MB	MO	RhB
-	90.0 min[a]	90 min[a]	90 min[a]
Natural zeolite (7)	90 min[a]	90 min[a]	90 min[a]
Ag NPs/natural zeolite (7)	21 min	8 min	17 min
Ag NPs/natural zeolite (7)[b]	9 min	3 min	7 min
Ag NPs/natural zeolite (7)[c]	20 min[a]	3 min	20 min[a]
Pd NPs/natural zeolite (7)	5 s	50 s	70 s
Fe_3O_4/natural zeolite (7)	90 min[a]	90 min[a]	90 min[a]
Ag/Fe_3O_4/natural zeolite (7)	5 min	3.5 min	3 min
Ag/Fe_3O_4/natural zeolite (3)	9 min	6.5 min	6 min
Ag/Fe_3O_4/natural zeolite (7)[b]	2 min	2 min	1 min
Pd/Fe_3O_4/natural zeolite (7)	3 s	5 s	55 s
Pd/Fe_3O_4/natural zeolite (3)	15 s	13 s	80 s
Pd/Fe_3O_4/natural zeolite (3)[c]	5 min[a]	3 s	5 min[a]
Pd/Fe_3O_4/natural zeolite (3)[d]	1.5 min	50 s	2 min

[a]No reaction; [b]$NaBH_4 = 10.6 \times 10^{-3}$ M; [c]pH = 3; [d]pH = 9.

Table 3. Comparison of the catalytic prowess of Ag/Fe_3O_4/natural zeolite and Pd/Fe_3O_4/natural zeolite with those of the reported catalysts for the RhB, MB, and MO reduction.

Dye	Catalyst	Time	Ref.
MO	Cu@SBA-15	5 min	[73]
	Ag NPs/seashell	11 min	[10]
	Ag–Ni/TP	15 min	[74]
	Ag/Fe_3O_4/natural zeolite	3.5 min	This work
	Pd/Fe_3O_4/natural zeolite	5 s	This work
RhB	Fe_3O_4@PANI@Au	18 min	[75]
	SiNWAs-Cu	14 min	[76]
	Silver nanoparticles	9 min	[77]
	Ag/Fe_3O_4/natural zeolite	3 min	This work
	Pd/Fe_3O_4/natural zeolite	55 s	This work
MB	CuNPs@NCC	12 min	[78]
	Au/CeO_2-TiO_2 nano-hybrid	10.5 min	[79]
	Au/Fe_3O_4@C composite	10 min	[80]
	Ag/Fe_3O_4/natural zeolite	5 min	This work
	Pd/Fe_3O_4/natural zeolite	3 s	This work

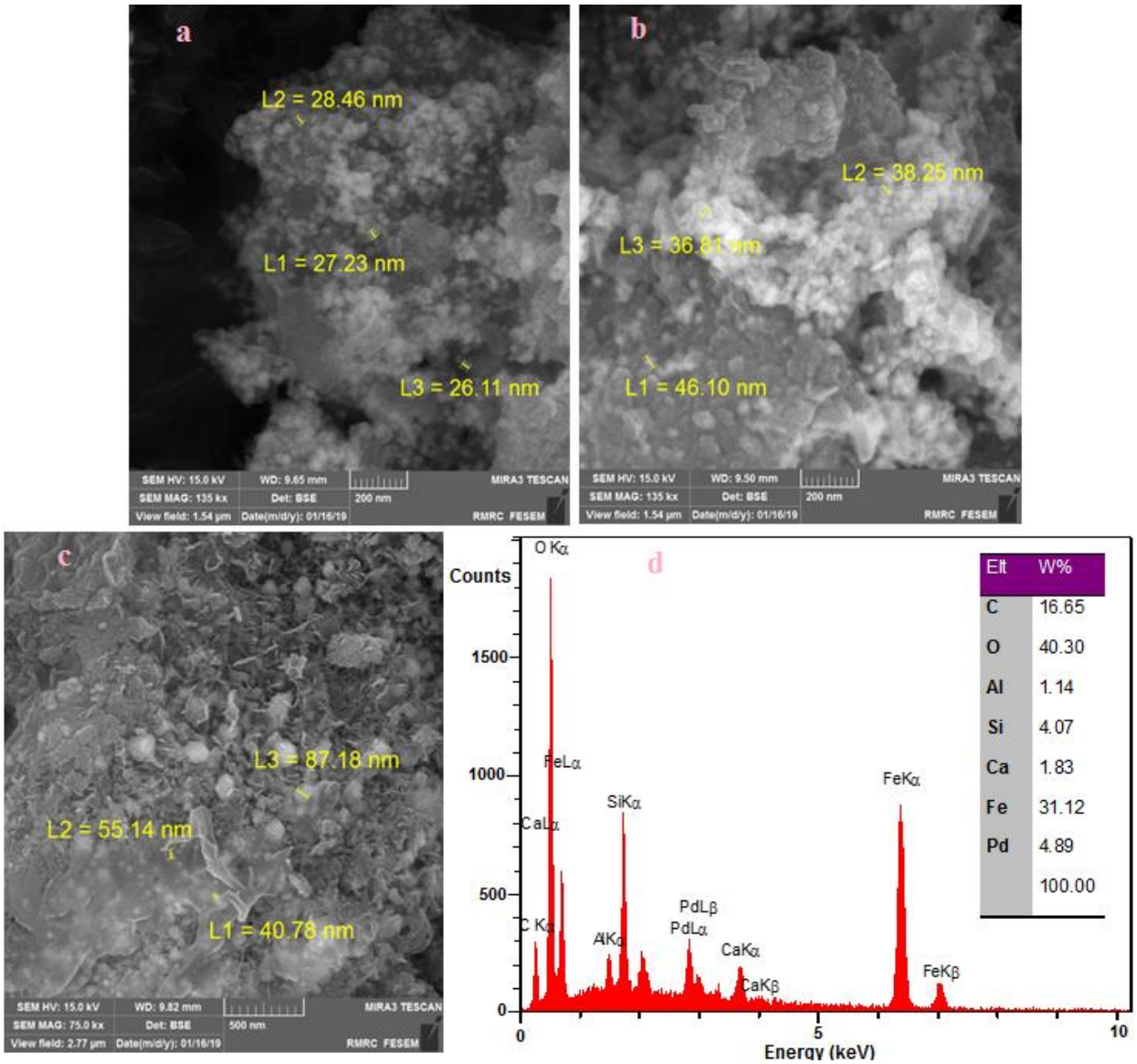

Fig. 11 (a-c) FESEM images and (d) EDS spectrum of the recycled Pd/Fe_3O_4/natural zeolite.

4. Conclusions

In this work, well-dispersed spherically shaped Ag and Pd nanoparticles were supported on the natural zeolite and its Fe_3O_4 nanocomposite as stable supports using aqueous *C. morifolium* flower extract. The formation of spherical Ag and Pd NPs with diameter below 60 nm was confirmed by different conventional techniques such as XRD, FESEM, EDS, and ICP-MS. These immobilized MNPs on the supports surfaces will be able to relay the electrons from BH_4^- ions to dye molecules and increase the reduction/decolorization efficiency of dyes. In opposite to that of MO, the reduced forms of RhB and MB can be oxidized again at the end of the reduction process and the colorless dyes solutions return to the original forms. Reusability test of the Pd/Fe_3O_4/natural zeolite nanocomposite exhibited the Pd loading and morphology of NPs of recycled catalyst are approximately unchanged on the support surface after 4 catalytic runs.

Acknowlegment

The authors thanks the NSTRI and University of Qom for financial supports of this work.

References

[1] B. Jaleh, M.G. Rouzbahani, K. Abedi, S. Azizian, H. Ebrahimi, M. Nasrollahzadeh, R.S. Varma, Clean Technol. Envir. 1-10.

[2] K.B. Tan, M. Vakili, B.A. Horri, P.E. Poh, A.Z. Abdullah, B. Salamatinia, Sep. Purif. Technol. 150 (2015) 229-242.
[3] S. Kavitha, M. Umadevi, S. Janani, T. Balakrishnan, R. Ramanibai, Spectrochim Acta A 127 (2014) 115-121.
[4] F. Torkamani, S. Azizian, J. Mol. Liq. 214 (2016) 270-275.
[5] D. Ke, J. Wang, H. Zhang, Y. Li, L. Zhang, X. Zhao, S. Han, Int. J. Hydrogen Energ. 42 (2017) 26617-26625.
[6] D. Lamey, O. Beswick, F. Cárdenas-Lizana, P.J. Dyson, E. Sulman, L. Kiwi-Minsker, Appl. Catal. A Gen. 542 (2017) 182-190.
[7] M.G. Goudarzi, M. Bagherzadeh, F. Taheri, A. Rostami-Vartooni, SN Appl. Sci. 2 (2020) 1-8.
[8] B. Khodadadi, M. Bordbar, M. Nasrollahzadeh, J. Collo. Interf. Sci. 490 (2017) 1-10.
[9] A. Molnar, Efficient, Chem. Rev. 111 (2011) 2251-2320.
[10] A. Rostami-Vartooni, M. Nasrollahzadeh, M. Alizadeh, J. Collo. Interf. Sci. 470 (2016) 268-275.
[11] A. Rostami-Vartooni, M. Nasrollahzadeh, M. Alizadeh, J. Allo. Compd. 680 (2016) 309-314.
[12] M. Amir, U. Kurtan, A. Baykal, Chin. J. Catal. 36 (2015) 1280-1286.
[13] H. Veisi, J. Gholami, H. Ueda, P. Mohammadi, M. Noroozi, J Mol. Catal. A Chem. 396 (2015) 216-223.
[14] M. Atarod, M. Nasrollahzadeh, S.M. Sajadi, J. Collo. Interf. Sci. 465 (2016) 249-258.
[15] B.M. Reddy, A. Khan, Catal. Rev. 47 (2005) 257-296.
[16] V. Pareek, A. Bhargava, R. Gupta, N. Jain, J. Panwar, Adv. Sci. Eng. Med. 9 (2017) 527-544.
[17] C.D. De Souza, B.R. Nogueira, M.E.C. Rostelato, J. Allo. Compd. 789 (2019) 714-740.
[18] A. Rostami-Vartooni, M. Nasrollahzadeh, M. Salavati-Niasari, M. Atarod, J. Allo. Compd. 689 (2016) 15-20.
[19] A. Rostami-Vartooni, A. Moradi-Saadatmand, M. Bagherzadeh, M. Mahdavi, Iran. J. Catal. 9 (2019) 27-35.
[20] M. Nasrollahzadeh, M. Maham, A. Rostami-Vartooni, M. Bagherzadeh, S.M. Sajadi, RSC Adv. 5 (2015) 64769-64780.
[21] I.S. Kim, S. Koppula, P.-J. Park, E.H. Kim, C.G. Kim, W.S. Choi, K.H. Lee, D.-K. Choi, J. Ethnopharmacol. 126 (2009) 447-454.
[22] O.A. Lawal, I.A. Ogunwande, O.F. Olorunloba, A. Oloku, Am. J. Essen. Oil. Nat. Prod. 2 (2014) 63-66.
[23] C.-K. Lii, Y.-P. Lei, H.-T. Yao, Y.-S. Hsieh, C.-W. Tsai, K.-L. Liu, H.-W. Chen, J. Ethnopharmacol. 128 (2010) 213-220.
[24] M. Ukiya, T. Akihisa, K. Yasukawa, Y. Kasahara, Y. Kimura, K. Koike, T. Nikaido, M. Takido, J. Agr. Food Chem. 49 (2001) 3187-3197.
[25] G.-H. Lin, L. Lin, H.-W. Liang, X. Ma, J.-Y. Wang, L.-P. Wu, H.-D. Jiang, I.C. Bruce, Q. Xia, J. Med. Food, 13 (2010) 306-311.
[26] P.-D. Duh, Food Chem. 66 (1999) 471-476.
[27] M. Ukiya, T. Akihisa, H. Tokuda, H. Suzuki, T. Mukainaka, E. Ichiishi, K. Yasukawa, Y. Kasahara, H. Nishino, Cancer Lett. 177 (2002) 7-12.
[28] J.S. Lee, H.J. Kim, Y.S. Lee, Plan. Med. 69 (2003) 859-861.
[29] C.W. Beninger, M.M. Abou-Zaid, A.L. Kistner, R.H. Hallett, M.J. Iqbal, B. Grodzinski, J.C. Hall, J. Chem. Ecol. 30 (2004) 589-606.
[30] Q. Guo, T. Wang, L. Cheng, J. Wen, T. Wang, Y. Liang, J. Chin. Mater. Med. 33 (2008) 756-759, 779.
[31] G. Tsitsishvili, Natural zeolites, Ellis Horwood Limited1992.
[32] D.W. Ming, E.R. Allen, Rev. Miner. Geochem. 45 (2001) 619-654.
[33] R. Barer, Zeolites and clay minerals as sorbent and molecular sieves, Academic Press, New York, 1987.
[34] M.R. Eskandarian, M. Fazli, M.H. Rasoulifard, H. Choi, Appl. Catal. B Environ. 183 (2016) 407-416.
[35] K. Shameli, M.B. Ahmad, M. Zargar, W.M.Z.W. Yunus, N.A. Ibrahim, Int. J. Nanomed. 6 (2011) 331-341.
[36] E. Kolobova, A. Pestryakov, A. Shemeryankina, Y. Kotolevich, O. Martynyuk, H.T. Vazquez, N. Bogdanchikova, Fuel, 138 (2014) 65-71.
[37] J. Behin, E. Ghadamnan, H. Kazemian, Clay Miner. 54 (2019) 131-144.
[38] A. Nezamzadeh-Ejhieh, M. Khorsandi, Iran. J. Catal. 1 (2011) 99-104.
[39] A. Nezamzadeh-Ejhieh, Z. Banan, Iran. J. Catal. 2 (2012) 79-83.
[40] A. Nezamzadeh-Ejhieh, M. Karimi-Shamsabadi, Chem. Eng. J. 228 (2013) 631-641.
[41] J. Talat-Mehrabad, M. Partovi, F. Arjomandi Rad, R. Khalilnezhad, Iran. J. Catal. 9 (2019) 233-239.
[42] K.A. Isai, V.S. Shrivatava, Iran. J. Catal. 9 (2019) 259-268.
[43] M.H. Habibi, E. Askari, Iran. J. Catal. 1 (2011) 41-44.
[44] L. Vafayi, S. Gharibe, Iran. J. Catal. 5 (2015) 365-371.
[45] M. Zebardast, A. Fallah Shojaei, K. Tabatabaeian, Iran. J. Catal. 8 (2018) 297-309.
[46] A. Rostami-Vartooni, A. Moradi-Saadatmand, M. Bagherzadeh, M. Mahdavi, Iran. J. Catal. 9 (2019) 27-35.

[47] M. Balakrishnan, R. John, Iran. J. Catal. 10 (2020) 1-16.
[48] A. Mahmoodi, S.M. Mehdinia, A. Rahmani, H. Nassehinia, Iran. J. Catal. 10 (2020) 23-32.
[49] N. Pourshirband, A. Nezamzadeh-Ejhieh, S.N. Mirsattari, Spectrochim. Acta A Mol. Biomol. Spec. 248 (2021) 119110-119128.
[50] A. Nezamzadeh-Ejhieh, N. Moazzeni, J. Ind. Eng. Chem. 19 (2013) 1433-1442.
[51] A. Nezamzadeh-Ejhieh, M. Karimi-Shamsabadi, Appl. Catal. A Gen. 477 (2014) 83-92.
[52] M. Karimi-Shamsabadi, A. Nezamzadeh-Ejhieh, J. Mol. Catal. A Chem. 418 (2016) 103-114.
[53] S. Ghattavi, A. Nezamzadeh-Ejhieh, Int. J. Hydrogen Energ., 45 (2020) 24636-24656.
[54] G. Panthi, M. Park, H.-Y. Kim, S.-Y. Lee, S.-J. Park, J. Ind. Eng. Chem. 21 (2015) 26-35.
[55] G. Zhang, X. Zhang, Y. Meng, G. Pan, Z. Ni, S. Xia, Chem. Eng. J. 392 (2020) 123684.
[56] J.A. Lercher, C. Gründling, G. Eder-Mirth, Catal. Today, 27 (1996) 353-376.
[57] D. Sternik, M. Majdan, A. Deryło-Marczewska, G. Żukociński, A. Gładysz-Płaska, V. Gun'Ko, S. Mikhalovsky, J. Therm. Anal. Calorim. 103 (2010) 607-615.
[58] C. Yang, Y. Guan, J. Xing, J. Liu, G. Shan, Z. An, H. Liu, Aiche J. 51 (2005) 2011-2015.
[59] N. Arabpour, A. Nezamzadeh-Ejhieh, Mater. Sci. Semicon. Proc. 31 (2015) 684-692.
[60] K. Elaiopoulos, T. Perraki, E. Grigoropoulou, A. Poulou, Microp. Mesopor. Mater. 134 (2010) 29-43.
[61] E. Karaoğlu, A. Baykal, M. Şenel, H. Sözeri, M.S. Toprak, Mater. Res. Bull. 47 (2012) 2480-2486.
[62] V. Ramasamy, P. Anand, G. Suresh, Adv. Powder Technol. 29 (2018) 818-834.
[63] E.M. Olegario, C.M.O. Pelicano, L.A. Dahonog, H. Nakajima, Mater. Res. Exp. 6 (2018) 015005.
[64] M. Minceva, R. Fajgar, L. Markovska, V. Meshko, Sep. Sci. Technol. 43 (2008) 2117-2143.
[65] Y. Zhang, W. Yan, Z. Sun, X. Li, J. Gao, RSC Adv. 4 (2014) 38040-38047.
[66] R. Wu, J.-H. Liu, L. Zhao, X. Zhang, J. Xie, B. Yu, X. Ma, S.-T. Yang, H. Wang, Y. Liu, J. Environ. Chem. Eng. 2 (2014) 907-913.
[67] N. Pourshirband, A. Nezamzadeh-Ejhieh, S.N. Mirsattari, Chem. Phys. Lett. 761 (2020) 138090.
[68] C.-H. Liu, X.-Q. Chen, Y.-F. Hu, T.-K. Sham, Q.-J. Sun, J.-B. Chang, X. Gao, X.-H. Sun, S.-D. Wang, ACS Appl. Mater.Interf. 5 (2013) 5072-5079.
[69] X.-L. Cai, C.-H. Liu, J. Liu, Y. Lu, Y.-N. Zhong, K.-Q. Nie, J.-L. Xu, X. Gao, X.-H. Sun, S.-D. Wang, Nano-Micro lett. 9 (2017) 1-10.
[70] M. Nasrollahzadeh, S.M. Sajadi, A. Rostami-Vartooni, M. Bagherzadeh, J. Collo. Interf. Sci. 448 (2015) 106-113.
[71] T. Nguyen Thi Thu, N. Nguyen Thi, V. Tran Quang, K. Nguyen Hong, T. Nguyen Minh, N. Le Thi Hoai, J. Exper. Nanosci. 11 (2016) 226-238.
[72] H.-J. Cui, H.-Z. Huang, B. Yuan, M.-L. Fu, Geochem. T. 16 (2015) 1-8.
[73] B.K. Ghosh, S. Hazra, B. Naik, N.N. Ghosh, Powder Technol. 269 (2015) 371-378.
[74] M. Ismail, M. Khan, S.A. Khan, M. Qayum, M.A. Khan, Y. Anwar, K. Akhtar, A.M. Asiri, S.B. Khan, J. Mater. Sci. Mater. El. 29 (2018) 20840-20855.
[75] S. Xuan, Y.-X.J. Wang, J.C. Yu, K.C.-F. Leung, Langmuir, 25 (2009) 11835-11843.
[76] X. Yang, H. Zhong, Y. Zhu, H. Jiang, J. Shen, J. Huang, C. Li, J. Mater. Chem. A, 2 (2014) 9040-9047.
[77] R. Vinayagam, T. Varadavenkatesan, R. Selvaraj, Green Process. Synth. 7 (2018) 30-37.
[78] A. Musa, M.B. Ahmad, M.Z. Hussein, M.I. Saiman, H.A. Sani, Res. Chem. Intermediat. 43 (2017) 801-815.
[79] P. Saikia, A. T MIAH, P.P. Das, J. Chem. Sci. 129 (2017) 81-93.
[80] Z. Gan, A. Zhao, M. Zhang, W. Tao, H. Guo, Q. Gao, R. Mao, E. Liu, Dalton T, 42 (2013) 8597-8605.